Benchmarking of the Characteristics Method Combined with Advanced Self-Shielding Models on BWR-MOX Assemblies

Romain Le Tellier*†, Alain Hébert†, Alain Santamarina‡ and Olivier Litaize‡
†*École Polytechnique de Montréal, C.P. 6079 succ. "Centre-Ville", Montréal CANADA H3C 3A7*
‡*CEA Cadarache DEN/DER/SPRC - Bldg. 230, 13108 Saint Paul-lez-Durance FRANCE*

Abstract

Calculations based on the characteristics method and different self-shielding models are presented for 9×9 BWR assemblies fully loaded with MOX fuel. The geometry of these assemblies was recovered from the BASALA experimental program implemented in the EOLE facility at CEA Cadarache. We have focused our study on two configurations, a "hot case" simulating hot operation conditions and a "cold case" with a cruciform control blade filled with B_4C poisoned rods.
A parametric study was carried out with respect to the spatial discretization, the tracking parameters and the anisotropy order. Comparisons with Monte-Carlo calculations in terms of k_{eff}, radiative capture and fission rates were performed in order to validate the computational tools. The results are in good agreement between the stochastic and deterministic approaches. The mutual self-shielding model recently introduced within the framework of the Ribon extending self-shielding method appears as useful for this type of assemblies. Indeed, in the calculation of these MOX benchmarks, the overlapping of resonances especially between ^{238}U and ^{240}Pu plays an important role due to the spectral strengthening of the flux as the voiding percentage is increased. The method of characteristics and the developed acceleration strategies are shown to be adequate to perform accurate calculations for these configurations handling a fine spatial discretization.

KEYWORDS: BWR, MOX, BASALA, self-shielding models, method of characteristics

1. Introduction

The benchmarks are assemblies recovered from the BASALA mock-ups program [1,2] i.e. 9×9 BWR assemblies fully loaded with MOX fuels with four different plutonium contents (3 %, 4.3 %, 7 %, 8.7 %) as shown on Figure 1. Each fuel pin has a zircaloy clad and a thin aluminum overclad. The isotopic compositions are slightly different from the experimental program but the basic design features and simulated physical properties as presented in Table 1 remain unchanged.

*Corresponding author, E-mail: romain.le-tellier@polymtl.ca

Figure 1: MOX distribution

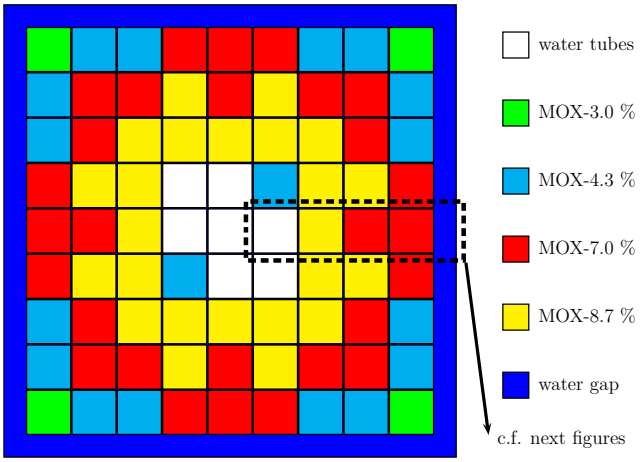

Table 1: Assemblies properties

	BASALA-HOT	BASALA-COLD
pitch	1.13	1.35
H/HM†	≈ 5	≈ 9
T	≈ 287 ^{o}C*	≈ 20 ^{o} C
p	≈ 75 bars*	≈ 1 bar
void fraction	≈ 42 %*	≈ 0 %

† hydrogen to heavy metal ratio
* simulated operating conditions

These assemblies simulate high moderation BWR in different operating conditions. We have studied two configurations: the BASALA-HOT assembly which represents hot conditions with 40 % voiding and the BASALA-COLD assembly for simulating higher moderation conditions along with a cruciform control blade filled with B_4C poisoned rods.

With this paper, we propose to validate a lattice calculations approach based on the characteristics method combined with different self-shielding models. These methods are part of a development version of the DRAGON lattice code. [3] The validation is performed by comparisons with Monte-Carlo calculations using the TRIPOLI4 code [4] both in terms of k_{eff} and integrated reactions rates.

2. The Computational Methods

The method of characteristics has been the subject of important investigations at École Polytechnique de Montréal. [5–7] This method can be used for lattice calculations as a transport solver in the self-shielding, leakage and multigroup flux solution components of the lattice code. [8]

The BWR-related calculations we are presenting are based on a custom implementation of this method that uses a variant of the algebraic collapsing acceleration proposed by Igor Suslov in the code MCCG3D. [9] These capabilities are available in development versions of the DRAGON code as presented in Ref. 10. However, the construction of the tracking information for BWR assemblies differs from the technique used for the CANDU 2D cell and 3D supercell of Ref. 10.

The basic geometry of a BWR assembly is a complicated two-dimensional geometry with irregular components representing water holes and control rods. Here, we have chosen to generate the track lengths using the TDT methodology developed by the Commissariat à l'Énergie Atomique. [11, 12] First, the geometry is analyzed in such a way to produce a set of *surface related elements*, each them representing an elementary segment or an arc of circle together with the neighboring regions indices. This decomposition in *surface related elements* is next analyzed to produce the tracking information relative to the integration lines crossing the assembly as a function of the spatial and angular quadrature parameters. A module was written in DRAGON to convert a TDT tracking file into the DRAGON format of the EXCELT: module. The TDT approach was selected in order to study the cruciform control blade which cannot be analyzed by the actual EXCELT: module of DRAGON.

Concerning the self-shielding models, five different approaches have been tested. Three of them are based on the improved Stamm'ler method as proposed in Ref. 13 with optional Nordheim distributed self-shielding model and Riemann integration model proposed in Ref. 14. The two others are based on a subgroup flux equation with probability tables. [15] The Ribon extended self-shielding model uses mathematical probability tables computed with a moment approach whereas the statistical self-shielding model is based on physical probability tables computed by fitting dilution-dependent cross sections. With both these models, the subgroup flux equation can be solved using the method of characteristics. Moreover, in the context of the Ribon extended approach, it was possible to test the mutual self-shielding model proposed in Ref. 15.

3. Description of the Treatment of BWR Assemblies

The fuel rods are distributed over a 9×9 grid as depicted on Fig. 1. Each fuel rod is split into 4 rings representing (inner to outer) respectively 50%, 30%, 15% and 5% of the rod volume according to the recommendation of Ref. 16 in order to treat correctly the spatial distribution of the resonant absorption of ^{238}U. The geometries of the two configurations we are interested in are depicted in Fig. 2; the relative scale between the two assemblies is shown.

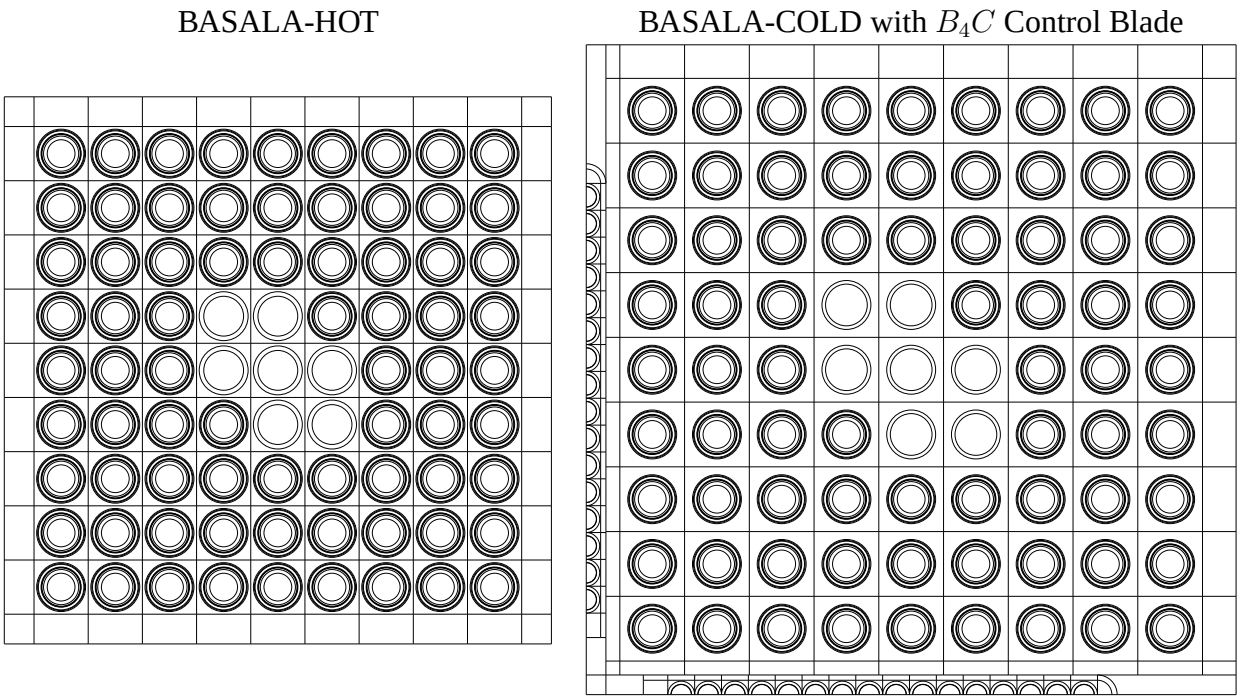

Figure 2: Modeled geometries

A simplified discretization is sufficient for performing the self-shielding calculation with the method of collision probabilities or with the method of characteristics. No mesh-splitting in the coolant region and white boundary conditions were used. Moreover, a coarser angular and spatial tracking was introduced without compromising the accuracy of the lattice calculation. The cells were grouped according to their Pu content.

Due to a small mean free path of neutrons in the coolant, an important refinement of both the geometry and the tracking is required for the multigroup calculation using the characteristics method based on a "flat-source approximation" for the flux integration. We observe the need to introduce mesh-splitting, sectorization and specular reflection using a cyclic tracking in order to avoid as far as possible any bias in the representation of the flux gradients. The parametric study in the BASALA-HOT configuration is presented in the next section. Besides, convergence with respect to the anisotropy order for the expansion of the scattering cross section is studied. We end up for the self-shielding models comparison with a configuration that is producing almost asymptotic results. As our goal was to validate methods, no attempt was performed to find a trade-off as one can find in the development of a computational scheme but this work is the basis of such a development.

For cross sections, we create a library in the DRAGON format, built from JEF-2.2 with NJOY [17] release 99.90 and the Dragr module. [18] This library is produced in the XMAS (172 groups) format and includes Autolib data for all the resonant isotopes between 2.76792 eV and 677.2873 eV. The PENDF files obtained in building this library were used for TRIPOLI4 calculations. Our TRIPOLI4 calculations are not using probability tables and, consequently, cannot represent unresolved self-shielding effects. In order to be consistent, we have disabled the self-shielding treatment in DRAGON for all groups lower than 45 corresponding to an energy greater than 11.138 KeV (i.e. for the unresolved resonances domain).

4. BASALA-HOT Numerical Results

In this section, we focus on the BASALA-HOT case. The relevant aspects of the parametric study are reported and the comparison with TRIPOLI4 is carried out with the different self-shielding models.

4.1 Notations and Configurations

The geometry discretization was studied from two points of view, the sectorization of the fuel cells and the coolant splitting. The configurations as depicted in Figs. 3 and 4 are referred by $\mathcal{F}_i$ and $\mathcal{C}_i$ respectively.

The tracking procedure is based on a cyclic azimuthal quadrature which approaches a uniform distribution of angles in $[0, \pi/2]$ [12] and a constant spatial step. The polar quadrature is obtained by a Bickley Naylor optimization procedure as proposed in Ref. 19.

Concerning the anisotropic scattering, P_L will be used to refer to an expansion of the scattering cross section in Legendre polynomials up to order L. Moreover, P_0^* and $P_0^\dagger$ denote respectively the APOLLO- and WIMS-type transport corrections for the isotropic scattering cross sections. [3]

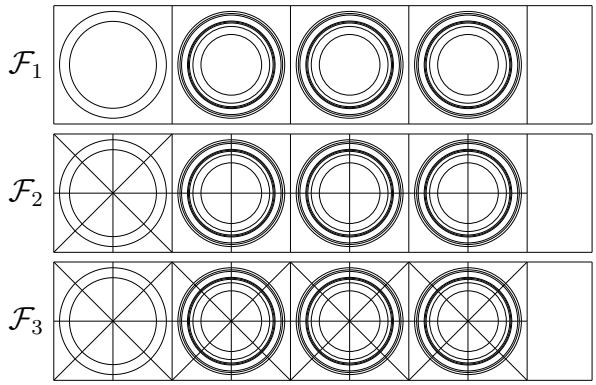

Figure 3: Cell sectorization configurations

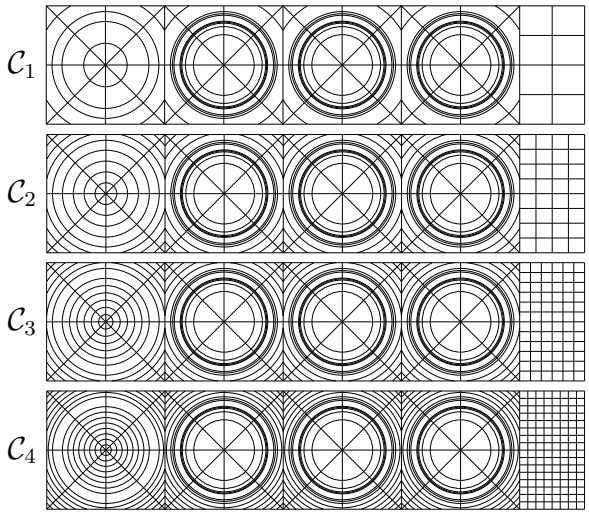

Figure 4: Coolant splitting configurations

The five self-shielding approaches will be referred by USS 1, USS 2, SHI 0, SHI 1, SHI 2 and correspond respectively to

- USS 1: a self-shielding calculation for isotopes ^{235}U, ^{238}U, ^{238}Pu, ^{239}Pu, ^{240}Pu, ^{241}Pu, ^{242}Pu,^{241}Am and Zr using the Ribon extended model in groups where Autolib data is available and the statistical model in the other resonant groups. In USS 1*, the mutual self-shielding effect is taken into account for ^{238}U and ^{240}Pu; we focus on these isotopes because of the overlapping of their resonances around 66 eV and 21 eV.
- USS 2: a self-shielding calculation for isotopes ^{235}U, ^{238}U, ^{238}Pu, ^{239}Pu, ^{240}Pu, ^{241}Pu, ^{242}Pu,^{241}Am and Zr using the statistical model in all resonant groups.
- SHI 0: the improved Stamm'ler method with Livolant-Jeanpierre normalization. This is the only self-shielding model available in DRAGON Release 3.
- SHI 1: SHI 0 with the Nordheim (PIC) distributed self-shielding model.
- SHI 2: SHI 0 with both Nordheim (PIC) distributed self-shielding model and Riemann integration method.

According to these notations, the starting configuration for the different analysis is a P_0^* scattering treatment with the USS 1* self-shielding model; it uses the $\mathcal{C}_4$-$\mathcal{F}_3$ geometry and a tracking procedure with a spatial step of 0.01cm, 8 azimuthal angles in $[0, \pi/2]$ and 2 polar angles.

We present the results in terms of the difference in k_{eff} i.e $\delta k_{\text{eff}} = k_{\text{eff}} - k_{\text{eff}}^{\text{ref.}}$ and the average ($\bar{\epsilon}$) and maximum (ϵ_{max}) differences on macroscopic reaction rates (τ) per cell. These differences are defined as

$$|\epsilon_{\text{max}}| = \max_i \left(\frac{|\tau_i - \tau_i^{\text{ref.}}|}{\tau_i^{\text{ref.}}} \right), \quad (1)$$

$$\bar{\epsilon} = \frac{1}{V_{\text{tot}}} \sum_i V_i \frac{|\tau_i - \tau_i^{\text{ref.}}|}{\tau_i^{\text{ref.}}}. \quad (2)$$

For this comparison, the reaction rates are condensed into 4 groups as presented in Table 2, based on a decomposition into fast, resonant (unresolved/resolved), thermal regions. For the parametric study, we focus on the fission rate in group 4, on the radiative capture rate in groups 2 and 3 and finally, on the total interaction rate in group 1.

Table 2: Macro energy groups for condensation

group	energy interval (eV)
1	$]4.0762.10^5$ $[$
2	$]6.7729.10^2$ $4.0762.10^5[$
3	$]2.7679$ $6.7729.10^2[$
4	$]$ $2.7679[$

The TRIPOLI4 calculations were carried out with 20000 batches and 1000 neutrons per batch, i.e. 20 millions histories. The standard deviation on the k_{eff} is about 25 pcm while it is about 0.1 % for the fission rate in group 4, 0.2 % and 0.4 % for the capture rate in group 2 and 3 respectively and 0.05 % on the total interaction rate in group 1.

4.2 Spatial Convergence

In Table 3, cell sectorizations $\mathcal{F}_1$ and $\mathcal{F}_2$ are compared with the $\mathcal{F}_3$ configuration. We clearly see that sectorization $\mathcal{F}_3$ is necessary in order to represent correctly the flux gradients within the assembly, especially in the thermal region.

Table 3: Sectorization effect

Fuel Cell Sectorization	Δk_{eff} (pcm)	$\bar{\epsilon}$ ($\epsilon_{\max}$) (%)							
		Fission gr. 4		Capture gr. 3		Capture gr. 2		Total gr. 1	
$\mathcal{F}_1$	311.7	2.24	(-4.41)	0.04	(0.05)	0.04	(-0.10)	0.41	(-0.91)
$\mathcal{F}_2$	64.3	0.45	(-0.94)	0.00	(-0.01)	0.01	(-0.02)	0.08	(-0.19)

Reference is taken as the $\mathcal{F}_3$ configuration

The effect of the coolant meshing is presented in Table 4 by comparing $\mathcal{C}_1$, $\mathcal{C}_2$ and $\mathcal{C}_3$ configurations with $\mathcal{C}_4$. A fine meshing is required to ensure the convergence of the thermal flux and the reactivity; $\mathcal{C}_3$ gives converged results.

Table 4: Coolant splitting convergence

Coolant Splitting	Δk_{eff} (pcm)	$\bar{\epsilon}$ ($\epsilon_{\max}$) (%)							
		Fission gr. 4		Capture gr. 3		Capture gr. 2		Total gr. 1	
$\mathcal{C}_1$	120.1	0.09	(0.17)	0.00	(0.01)	0.01	(0.01)	0.01	(-0.03)
$\mathcal{C}_2$	21.5	0.05	(0.08)	0.01	(0.01)	0.01	(0.02)	0.01	(0.01)
$\mathcal{C}_3$	-0.3	0.04	(0.04)	0.01	(0.01)	0.02	(0.02)	0.01	(0.01)

Reference is taken as the $\mathcal{C}_4$ configuration

Towards the definition of a computational scheme, the coolant splitting can be differentiated per cell. As observed in Ref. 20, a fine mesh is mandatory in the water gap between the assemblies and in the corner cells but within the assembly, a coarser mesh can be used.

4.3 Azimuthal Angle Convergence

Table 5 compares 8, 16, 20 angle calculations with respect to the 32 angle calculation. We clearly see that 20 angles guarantee properly converged results both in terms of reactivity and fluxes.

Table 5: Azimuthal angle convergence

Number of Angles	Δk_{eff} (pcm)	$\bar{\epsilon}$ ($\epsilon_{\max}$) (%)							
		Fission gr. 4		Capture gr. 3		Capture gr. 2		Total gr. 1	
8	-182.8	0.19	(-0.43)	0.28	(0.36)	0.16	(0.21)	1.04	(-2.02)
16	-30.1	0.05	(-0.09)	0.01	(0.02)	0.04	(0.04)	0.17	(-0.21)
20	-1.2	0.04	(0.06)	0.01	(-0.03)	0.01	(0.02)	0.05	(-0.18)

Reference is taken as the 32 angles calculation

As mentioned earlier, a cyclic tracking treating exactly the reflective boundary conditions is necessary to obtain good results.

4.4 Scattering Anisotropy

An important aspect related to the scattering anisotropy treatment is the polar quadrature. As shown in Ref. 12, the usage of polar angles derived from a Bickley Naylor optimization leads to a non-conservative scheme when considering an anisotropy order ≥ 2. This is related to the poor integration of the Legendre polynomials by such quadratures. In practice, on these assemblies, as observed in Ref. 21, the discrepancy appears when the integration of the fourth Legendre polynomial is involved i.e. for an anisotropy order ≥ 4. Consequently, in this study limited to the third order, the usage of this quadrature was maintained.

The results are presented in Table 6 while varying the anisotropy order from 0 to 2 taking as reference the P_3 calculation. We see that the anisotropy effect is quite important and that contrarily to standard PWR calculations, for these BWR-MOX configurations, the difference between P_1 and P_2 calculations is not negligible.

Table 6: Scattering anisotropy effect

Anisotropy Order	Δk_{eff} (pcm)	$\bar{\epsilon}$ ($\epsilon_{\max}$) (%)							
		Fission gr. 4		Capture gr. 3		Capture gr. 2		Total gr. 1	
P_0	-47.1	2.41	(6.50)	0.90	(-1.86)	1.17	(1.61)	0.57	(0.85)
P_0^*	-80.5	0.45	(0.52)	0.22	(-0.63)	0.52	(0.71)	0.63	(-1.64)
$P_0^\dagger$	-74.2	0.34	(-0.43)	0.20	(-0.34)	0.71	(0.94)	0.41	(-1.13)
P_1	-128.4	0.19	(-0.25)	0.34	(0.45)	0.06	(0.21)	0.23	(-0.29)
P_2	30.4	0.02	(0.06)	0.06	(-0.06)	0.06	(-0.08)	0.11	(0.13)

Reference is taken as the P_3 configuration

4.5 Self-Shielding Models Comparison

According to the previous convergence studies, for the comparison of the different self-shielding models, the flux calculation was carried out using a P_2 scattering expansion on the discretized geometry $\mathcal{C}_3$-$\mathcal{F}_3$. The tracking procedure uses 20 azimuthal angles and 3 polar angles.

The results are presented in Table 7. They show the good agreement between DRAGON and TRIPOLI4 when using a subgroup approach for the self-shielding procedure. An interesting aspect is the improvement provided by the treatment of the mutual self-shielding between ^{238}U and ^{240}Pu which accounts for 134 pcm. Concerning the Stamm'ler method, the developments introduced by SHI 1 and 2 improve largely the k_{eff} prediction but reaction rates show the limits of such approaches.

If we look at the fission rate, we observe a very good agreement between DRAGON and TRIPOLI4 whatever the self-shielding model is. The average error is within three standard deviations of the TRIPOLI4 calculation. This result validates the treatment of the geometry with the characteristics method.

Table 7: Comparison between DRAGON and TRIPOLI4

Self-Shielding Model	Δk_{eff} (pcm)	$\bar{\epsilon}$ ($\epsilon_{\max}$) (%)							
		Fission gr. 4		Capture gr. 3		Capture gr. 2		Total gr. 1	
USS 1*	-71	0.26	(-0.60)	1.07	(1.39)	0.40	(-0.41)	0.89	(-1.19)
USS 1	-205	0.21	(-0.68)	1.79	(2.15)	0.40	(-0.41)	0.89	(-1.18)
USS 2	-204	0.21	(-0.68)	1.74	(2.06)	0.40	(-0.41)	0.89	(-1.18)
SHI 0	-464	0.23	(-0.64)	13.98	(14.17)	0.64	(-2.64)	0.89	(-1.14)
SHI 1	-300	0.46	(0.61)	3.24	(5.74)	4.91	(-5.80)	0.91	(-1.06)
SHI 2	-77	0.24	(-0.52)	3.73	(4.56)	4.90	(-5.82)	0.89	(-1.17)

TRIPOLI4 Reference k_{eff} is equal to 1.23933 ($\sigma = 26$pcm)

In Table 8 and 9, we presents some details in the comparison for the radiative capture in group 2 and 3 respectively. The homogenization is done over pincells sharing the same MOX concentration although the flux spectra are slightly different; no noticeable compensations are hidden by this choice in presenting the results. The 4 rings are not homogenized in order to highlight the rim effect and its representation depending on the self-shielding model. Consequently, the merged regions are referred as "MOX wt% i_r" where i_r corresponds to the annular region considered (i_r goes from 1 to 4 from inner region to outer region).

In group 2 corresponding to the unresolved resonances range, we see that USS 1 with or without correlation and USS 2 gives results very close to the TRIPOLI4 reference; most of the results are within two standard deviations and all of them are within three standard deviations. For SHI 0, we see a clear underestimation in the capture rate in all the outer rings of the pins because of the rim effect. SHI 1 and 2 gives close results which show an underestimation in the inner region of the pins and an overestimation in the outer region; these models overpredict the rim effect in this energy range. These results are coherent with what was observed on other types of assemblies. [8]

In the resolved resonances range, the situation is worse for SHI, the incapability of the SHI 0 formalism to take into account the spatial self-shielding distribution is clear and leads to large errors. With SHI 1 and 2, the results are greatly improved but the errors remain important in the outer region of the pins. When using USS 1 or 2, the results become close to TRIPOLI4. While USS 1 without correlation and USS 2 give similar results, the introduction of the mutual self-shielding model along with USS 1 reduces noticeably the error. It is interesting to note that while the Pu content of a cell increases, the discrepancy is increased as it is mostly due to the overlapping of ^{238}U and ^{240}Pu resonances. Relevant values illustrating this phenomenon and its improvement using the correlation model are underlined in Table 9.

Table 8: Radiative capture rate in macro-group 2

Merged Region	TRIPOLI4 Reaction Rate	ε (%) USS 1*	USS 1	USS 2	SHI 0	SHI 1	SHI 2
3.0% 1	9.59516e-04	-0.18	-0.18	**-0.18**	-0.87	-6.58	-6.60
3.0% 2	6.01239e-04	-0.07	-0.07	**-0.07**	-5.30	-5.65	-5.67
3.0% 3	3.14838e-04	0.47	0.47	0.47	-9.28	**-0.32**	-0.34
3.0% 4	1.08800e-04	**0.56**	0.56	0.56	-12.75	10.83	10.81
4.3% 1	4.41785e-03	-0.49	-0.49	-0.49	**0.11**	-6.25	-6.25
4.3% 2	2.75745e-03	-0.30	**-0.30**	-0.30	-3.69	-5.20	-5.21
4.3% 3	1.43661e-03	-0.14	**-0.14**	-0.14	-7.52	-0.46	-0.47
4.3% 4	4.95087e-04	0.05	0.05	**0.05**	-10.53	10.80	10.80
7.0% 1	7.13138e-03	**-0.46**	-0.46	-0.46	1.00	-5.52	-5.51
7.0% 2	4.42787e-03	**-0.31**	-0.31	-0.31	-2.27	-4.46	-4.46
7.0% 3	2.29078e-03	-0.32	-0.32	-0.32	-5.72	-0.08	**-0.08**
7.0% 4	7.85262e-04	0.05	0.05	**0.05**	-8.18	11.02	11.02
8.7% 1	6.27233e-03	**-0.47**	-0.47	-0.47	1.19	-5.23	-5.22
8.7% 2	3.88629e-03	**-0.33**	-0.34	-0.34	-1.92	-4.15	-4.14
8.7% 3	2.00898e-03	**-0.19**	-0.19	-0.19	-5.05	0.29	0.30
8.7% 4	6.88344e-04	**-0.12**	-0.12	-0.13	-7.63	10.93	10.94

Table 9: Radiative capture rate in macro-group 3

Merged Region	TRIPOLI4 Reaction Rate	ε (%) USS 1*	USS 1	USS 2	SHI 0	SHI 1	SHI 2
3.0% 1	3.16810e-03	**1.07**	1.70	1.56	22.80	7.23	3.52
3.0% 2	2.25222e-03	**0.57**	1.01	1.53	7.97	5.86	2.13
3.0% 3	1.56002e-03	0.69	0.92	1.60	-19.21	0.52	**-0.33**
3.0% 4	1.17163e-03	0.16	0.17	**0.11**	-63.53	-15.03	-14.12
4.3% 1	1.41355e-02	**1.00**	1.75	1.57	22.34	6.63	3.88
4.3% 2	9.90927e-03	**0.22**	0.76	1.10	9.20	5.14	2.19
4.3% 3	6.61854e-03	-0.21	**0.10**	0.56	-15.62	1.22	-0.92
4.3% 4	4.65656e-03	-1.05	**-1.03**	-1.15	-59.25	-14.90	-14.64
7.0% 1	2.31598e-02	**1.57**	2.43	2.22	21.41	3.58	5.09
7.0% 2	1.59881e-02	**0.71**	1.36	1.53	9.95	2.89	3.28
7.0% 3	1.03090e-02	-0.54	-0.16	**0.10**	-12.29	0.79	0.63
7.0% 4	6.66313e-03	-1.54	**-1.51**	-1.71	-53.86	-11.72	-12.65
8.7% 1	2.04708e-02	**1.85**	2.72	2.51	20.94	2.28	5.66
8.7% 2	1.40839e-02	**1.01**	1.67	1.80	9.82	1.58	3.89
8.7% 3	9.01504e-03	-0.36	**0.02**	0.24	-11.53	0.04	1.53
8.7% 4	5.63948e-03	-1.27	**-1.25**	-1.46	-51.99	-10.31	-11.14

In these calculations, the Algebraic Collapsing Acceleration was used as a preconditioner of the multigroup iterations and gave good results. All the calculations were converged with a total of 20 to 25 multigroup flux integrations.

5. BASALA-COLD Numerical Results

In this section, the BASALA-COLD configuration with the B_4C control blade is studied. The modeling is following the recommendation of the parametric studies performed on the BASALA-HOT assembly.

The results are presented in Table 10 for the USS 1 self-shielding model with and without the mutual self-shielding treatment between ^{238}U and ^{240}Pu. A good agreement between DRAGON and TRIPOLI4 is observed. When comparing with BASALA-HOT results, a noticeable difference is the degradation of the thermal fission rate prediction due to the presence of a strong absorber in the blade. However, this maximum error of 1.4% is totally acceptable, especially as the power of this cross-controlled assembly is largely reduced. Indeed, its peak power is not a safety issue.

Another interesting point is that the difference in k_{eff} between USS 1* and USS 1 is reduced from 134 pcm in the BASALA-HOT configuration to 73 pcm in this case. Indeed, this assembly simulates higher moderation conditions; consequently the flux spectrum is more thermal and the discrepancy introduced by the overlapping of resonances in the epithermal region is reduced.

Table 10: Comparison between DRAGON and TRIPOLI4

Self-Shielding Model	Δk_{eff} (pcm)	$\bar{\epsilon}$ (ϵ_{max}) (%)							
		Fission gr. 4		Capture gr. 3		Capture gr. 2		Total gr. 1	
USS 1*	-70	0.69	(1.40)	1.10	(1.54)	0.18	(-0.41)	0.98	(-1.18)
USS 1	-143	0.67	(1.35)	1.76	(2.04)	0.18	(-0.41)	0.98	(-1.18)

TRIPOLI4 Reference k_{eff} is equal to 1.12617 ($\sigma = 27$pcm)

6. Conclusions

In this paper, the usage of the characteristics method along with different self-shielding models was tested on BWR assemblies fully loaded with MOX fuel with different Pu contents. The comparison was performed in terms of k_{eff}, radiative capture rate and fission rate with Monte-Carlo calculations. The method of characteristics was found efficient for this kind of geometry with a high moderation ratio which requires a fine mesh, especially in the water gap between the assemblies. Concerning the self-shielding models, the subgroup approaches gave good results whereas the models based on the Stamm'ler method lead to a rather large discrepancy in the representation of the rim effect. Moreover, the mutual self-shielding effect, particularly between ^{238}U and ^{240}Pu has a noticeable effect in the reactivity of such assemblies and the mutual self-shielding model proposed recently in the context of the Ribon extended approach was found efficient in reducing the discrepancy induced by this phenomenon.

ACKNOWLEDGMENTS

The authors wish to thanks CEA, COGEMA, and NUPEC which founded the BASALA program.

References

1) S. Cathalau, P. Blaise, P. Fougeras, N. Thiollay, A. Santamarina, O. Litaize, T. Yamamoto, R. Kanda, M. Sasagawa, T. Umano, T. Kikuchi and J. L. Nigon, "High Moderation Boiling

Water Reactors fully loaded with MOX fuel : The BASALA Experimental Program", *Int. Mtg. on the Physics of Fuel Cycles and Advanced Nuclear Systems. PHYSOR 2004*, Chicago, April 25-29, 2004.

2) O. Litaize, A. Santamarina, M. Hervault, S. Cathalau, P. Fougeras, P. Blaise, T. Yamamoto, R. Kanda, M. Sasagawa and T. Kikuchi, "Monte Carlo Analysis of High Moderation 100% MOX BWR Cores using JEF2 and JENDL3 Nuclear Data", *Int. Mtg. on the Physics of Fuel Cycles and Advanced Nuclear Systems. PHYSOR 2004*, Chicago, April 25-29, 2004.

3) G. Marleau, A. Hébert and R. Roy, "A User's Guide for DRAGON", *Report IGE-174 Rev. 5*, Institut de Genie Nucléaire, École Polytechnique de Montréal (2000).

4) J. P. Both and Y. Peneliau, "The Monte Carlo code TRIPOLI-4 and its first benchmark interpretations", *Int. Conf. on the Physics of Reactors. PHYSOR 1996*, Mito, 1996.

5) G. J. Wu and R. Roy, "A new Characteristics algorithm for 3D transport calculations," *Ann. nucl. Energy.*, **30**, 1-16 (2003).

6) R. Le Tellier and A. Hébert, "Spectral Analysis of an Algebraic Collapsing Acceleration for the Characteristics Method", *Int. Mtg. in Mathematics & Computations, Supercomputing, Reactor Physics and Nuclear and Biological Applications. M&C 2005*, September 12-15, Avignon, 2005.

7) R. Le Tellier and A. Hébert, "Application of the DSA Preconditioned GMRES Formalism to the Method of Characteristics - First Results", *Int. Mtg. on the Physics of Fuel Cycles and Advanced Nuclear Systems: Global Developments. PHYSOR 2004*, Chicago, April 25-29, 2004.

8) R. Le Tellier and A. Hébert, "Application of the Characteristics Method Combined with Advanced Self Shielding Models to an ACR-Type Cell," *26th CNS Annual Conf.*, Toronto, June 13-15, 2005.

9) I. R. Suslov,"An Algebraic Collapsing Acceleration in Long Characteristics Transport Theory," *11th Symposium of AER on VVER Reactor Physics and Reactor Safety*, Csopak, September 24-28, Csopak, 2001.

10) R. Le Tellier, A. Hébert and G. Marleau, "The implementation of a 3D characteristics solver for the generation of incremental cross sections for reactivity devices in a CANDU reactor", this meeting.

11) R. Sanchez and L. Mao, "New Developments in the Interface-Current Module TDT", *Int. Conf. on Mathematical Methods and Supercomputing for Nuclear Applications. SNA 1997*, Saratoga Springs, October 5-9, 1997.

12) R. Sanchez, L. Mao and S. Santandrea, "Treatment of Boundary Conditions in Trajectory-Based Deterministic Transport Methods", *Nucl. Sc. Eng.*, **140**, 23-50 (2002).

13) A. Hébert and G. Marleau, "Generalization of the Stamm'ler Method for the Self-Shielding Resonant Isotopes in Arbitrary Geometries", *Nucl. Sc. Eng.* **108**, 230-239 (1991).

14) A. Hébert, "Revisiting The Stamm'ler Self-Shielding Model", *25th CNS Annual Conference*, Toronto, 2004.

15) A. Hébert, "The Ribon Extended Self-Shielding Model", *Nucl. Sc. Eng.*, **151**, 1-24 (2005).

16) A. Santamarina, C. Collignon and C. Garat, "French Calculation Schemes for Light Water Reactor Analysis", *Int. Mtg. on the Physics of Fuel Cycles and Advanced Nuclear Systems: Global Developments. PHYSOR 2004*, Chicago, April 25-29, 2004.

17) R. E. MacFarlane, D. W. Muir, “NJOY99.0 Code System for Producing Pointwise and Multigroup Neutron and Photon Cross Sections from ENDF/B Data”, *PSR-480/NJOY99.0*, Los Alamos National Laboratory (2000).

18) A. Hébert and H. Saygin, “Development of DRAGR for the Formatting of DRAGON Cross Section Libraries”, *Seminar on NJOY-91 and THEMIS for the Processing of Evaluated Nuclear Data Files*, Saclay, 1992.

19) A. Leonard, C. T. McDaniel, “Optimal Polar Angles and Weights for the Characteristics Method”, *Trans. Am. Nucl. Soc.*, **73**, 172-173, 1995.

20) A. Santamarina, N. Hfaiedh, R. Le Tellier, V. Marotte, S. Misu, A. Sargeni, C. Vaglio-Gaudard and I. Zmijarevic, “Advanced Neutronics Tools for BWR Design Calculations", *Int. Conf. on Nuclear Engineering. ICONE 14*, Miami, July 17-20, 2006.

21) C. Vaglio-Gaudard, A. Santamarina, A. Sargeni, R. Le Tellier and J. F. Vidal, “Qualification of APOLLO2 BWR calculation scheme on the BASALA mock-up", this meeting.